Magnetic anisotropy and anomalous Hall effect in monoclinic single crystal Cr_5Te_8

Z. Z. Jiang,[1,2] X. Luo,[1,*] J. Yan,[1,2] J. J. Gao,[1,2] W. Wang,[1,2] G. C. Zhao,[1,2] Y. Sun,[3] J. G. Si,[1,2] W. J. Lu,[1] P. Tong,[1] X. B. Zhu,[1] W. H. Song,[1] and Y. P. Sun[4,1,5,†]

[1]*Key Laboratory of Materials Physics, Institute of Solid State Physics, HFIPS, Chinese Academy of Sciences, Hefei 230031, China*
[2]*University of Science and Technology of China, Hefei 230026, China*
[3]*Institutes of Physical Science and Information Technology, Anhui University, Hefei 230601, China*
[4]*Anhui Province Key Laboratory of Condensed Matter Physics at Extreme Conditions, High Magnetic Field Laboratory, HFIPS, Chinese Academy of Sciences, Hefei 230031, China*
[5]*Collaborative Innovation Center of Advanced Microstructures, Nanjing University, Nanjing 210093, China*

(Received 15 January 2020; revised 30 September 2020; accepted 30 September 2020; published 22 October 2020)

Layered magnetic materials with nontrivial spin configurations usually emerge novel magnetic and transport properties. Herein, we investigate the anisotropy of magnetic properties and the anomalous Hall effect (AHE) in the layered itinerant ferromagnetic (FM) monoclinic Cr_5Te_8 (m-Cr_5Te_8) single crystal. There are some observations: (1) Based on the measurement of angular-dependent magnetization $M(\varphi)$, the system shows strong twofold out-of-plane symmetry. Meanwhile, the maximum of the rotational magnetic entropy change $\Delta S_M^{\mathrm{R}}(T,H)$ between the c axis and the ab plane is about 1.1 $\mathrm{J\,kg^{-1}\,K^{-1}}$ with a magnetic-field change of 4.5 T. Both indicate that there exists a strong uniaxial anisotropy in m-Cr_5Te_8. (2) The paramagnetic-FM phase-transition temperature (T_{C}) of m-Cr_5Te_8 is about 186 K and very sensitive to the applied pressure (P) with the derivative of T_{C} with respect to $P\,dT_{\mathrm{C}}/dP \sim -50\ \mathrm{K\,GPa^{-1}}$. (3) As to the AHE, by considering the scaling behavior between the anomalous Hall resistivity ρ_{xy}^{A} and the longitudinal resistivity ρ_{xx}, the origin of the AHE in m-Cr_5Te_8 can be described by the skew-scattering mechanism. Moreover, the measurements of the AHE and isothermal magnetization confirm that the spin-flop behavior exists in m-Cr_5Te_8. The critical field H_{C} is about 0.26 T, and a possible explanation is given with the magnetic phase diagram of m-Cr_5Te_8 drawn.

DOI: 10.1103/PhysRevB.102.144433

I. INTRODUCTION

Recently, two-dimensional (2D) materials have stimulated great interest due to their remarkable properties and immense potential in scalable device applications. However, spintronic devices based on 2D materials are still in the initial stage because long-range ferromagnetic (FM) order is strongly suppressed in 2D materials systems by thermal fluctuations, according to the Mermin-Wagner theorem [1]. Researchers have put a lot of effort into exploring the 2D magnetic materials. At first, through first-principles calculations, Li and Yang [2] demonstrated the possibility of realizing 2D FM semiconductors by exfoliating layered crystals of $CrXTe_3$ ($X =$ Si, Ge). The work of Zhang *et al.* [3] and McGuire *et al.* [4] suggest that monolayer CrX_3 ($X =$ F, Cl, Br, and I) are robust intrinsic FM materials with large magnetic moments. Until recent years, several 2D van der Waals (vdW) magnetic materials with intrinsic FM order have been experimentally found by a sophisticated exfoliation process [5,6]. For example, $Cr_2Ge_2Te_6$ is a layered material constructed from an ABAB hexagonal close packing of tellurium atoms [7]. A strong dimensionality effect has been revealed by scanning magneto-optic Kerr microscopy. With decreasing thickness, the paramagnetic (PM)-FM phase transition temperature (T_{C}) decreases monotonically from 68 K (bulk) to 30 K (bilayer) [8]. Similarly, CrI_3 is an Ising ferromagnet with the out-of-plane spin orientation. Its magnetism can persist in the monolayer with T_{C} of 45 K, which is slightly lower than that of bulk crystals ($T_{\mathrm{C}} = 61$ K). Interestingly, the magnetic ground state of CrI_3 can be tuned by thickness. The ferromagnetism in the monolayer, antiferromagnetism in the bilayer, and ferromagnetism in the trilayer have been observed [9]. Another typical example is Fe_3GeTe_2, its bulk T_{C} is about 205 K and can be suppressed in thin flakes. By applying a small grid voltage with lithium-ion inserting on Fe_3GeTe_2 thin layers, T_{C} can be raised to room temperature, much higher than the bulk [10], which may open up an opportunity for fundamental physics and gate tunable spintronics. Although all these materials present intrinsic FM behavior, the T_{C}s are lower than room temperature, restricting their potential applications. Batzill [11] *et al.* reported the emergence of FM order above room temperature for monolayer VSe_2 grown by molecular beam epitaxy on graphite. However, it is chemically unstable in air, which still limits the applications in spintronics devices. Therefore, exploring other new 2D magnetic materials is an important front in condensed-matter physics and material sciences.

Zhang [12] *et al.* have provided an ambient pressure chemical vapor deposition approach to controllably synthesize ultrathin Cr_nX ($X =$ S, Se, and Te; $0 < n < 1$) on mica substrates very recently. Chromium tellurides can be good candidates for their rich and adjustable physical prop-

*Corresponding author: xluo@issp.ac.cn
†ypsun@issp.ac.cn

erties. Chromium tellurides family $Cr_{1-x}Te$ ($0 < x < 0.667$) present FM behavior with layered structures. Depending on the composition of the Cr element, T_C changes from 170 to 360 K [13–15]. Their structures are based on the NiAs type by successive removal of Cr in every second metal atom layer parallel to c axis [16]. Some typical crystal phases [17] have been extensively studied: (i) hexagonal $Cr_{1-x}Te$ ($x < 0.1$). Berg [18] reported that stoichiometric CrTe does not exist with a random distribution of vacancies in alternate transition metal layers. It has a high T_C and a strong decrease in T_C with the pressure according to the study of Hatakeyama *et al.* [19]; (ii) monoclinic Cr_3Te_4 ($x = 0.25$). The T_C observed for Cr_3Te_4 is in the range of 315–340 K [13], and it presents negative magnetoresistance as well as anomalous Hall effect (AHE) behavior [20]; (iii) trigonal Cr_2Te_3 ($x = 0.333$). The ordered magnetic moment obtained by the measurement of the neutron diffraction is about 2.65–2.70μ_B which is smaller than the calculated 3.0μ_B due to possible spin canting and itinerant nature of Cr's 3d electrons [21]; (iv) monoclinic $CrTe_3$ ($x = 0.667$). It is a novel vdW material whose tellurium sublattice contains three entities as a polytelluride [22], and it shows significant magnetoelastic coupling [23]; (v) trigonal and monoclinic Cr_5Te_8 ($x = 0.375$). Cr_5Te_8 crystallizes a trigonal phase tr-Cr_5Te_8 at high temperatures, whereas a monoclinic phase m-Cr_5Te_8 at low temperatures. The T_C of Cr_5Te_8 is in the range of 180 to 230 K, sensitively depending on the concentration of Te [15]. For tr-Cr_5Te_8, it is stable in a relatively high concentration (61.5–62.5-at. % Te) than m-Cr_5Te_8 (59.6–61.5-at. % Te) [16,24]. It should be noted that a continuous transition between the two structures is improbable [17]. Although m-Cr_5Te_8 has a higher Cr concentration, it exhibits lower T_C, which can be explained on the basis of less effective FM superexchange interactions in the monoclinic compound and the larger number of Cr atoms being antiferromagnetically coupled [25]. Some work related to the magnetic and transport property have been extensively performed on tr-Cr_5Te_8 [14,26–29], but detailed investigations on m-Cr_5Te_8 are still incomplete.

In this paper, we grew single crystals and performed comprehensive investigations on the magnetic and the electronic transport properties of m-Cr_5Te_8. Large magnetic anisotropy and strong pressure dependence of T_C have been observed. Additionally, the linear scaling behavior between the anomalous Hall resistivity ρ_{xy}^{A} and the longitudinal resistivity ρ_{xx} confirms that the origin of AHE can be explained by the skew-scattering mechanism. Meanwhile, a novel sudden jump phenomenon induced by the magnetic field and temperature has also been observed, which might be related to a spin-flop process accompanied by a change of the magnetic structure. The possible magnetic structure and the magnetic phase diagram of m-Cr_5Te_8 were eventually obtained.

II. EXPERIMENTAL DETAILS

Single crystals of m-Cr_5Te_8 were grown by the mixed-flux method [30,31], and the molar ratio of Cr:Ge:Te is 1:6:10. A certain amount of Cr (purity 99.5%) powder, Ge (purity 99.99%) pieces, and Te (purity 99.999%) chunks was put into an alumina crucible and sealed in a quartz ampoule. The quartz ampoule was then heated to 1123 K and equilibrated for 10 h and cooled down to 723 K at the rate of 3 K/h in the next. Eventually, the ampoule was taken out quickly from the furnace and decanted with a centrifuge to separate crystals from the flux.

X-ray diffraction (XRD) of polycrystalline powders and single crystals were performed by the PANalytical X' Pert diffractometer using the Cu Kα radiation ($\lambda = 0.15406$ nm) at room temperature. The atomic ratio was determined by Aztec-X-Max 80 energy dispersive x-ray spectrometer in Hitachi SU8000 Series scanning electron microscope (Fig. S1 of the Supplemental Material [32]). Magnetization and electrical transport measurements were carried out by using the Quantum Design magnetic property measurement system (MPMS-XL5) and the physical properties measurement system (PPMS-9T). A seven-probe method was used for the longitudinal resistivity ρ_{xx} and the transverse Hall resistivity ρ_{xy} measurements of different temperatures and magnetic fields. The external magnetic fields were perpendicular to the ab plane and the current was along the ab plane. The Hall resistivity was obtained by the difference of transverse resistance measured in positive and negative fields (i.e., $\rho_{xy}(\mu_0 H) = [\rho_{xy}(+\mu_0 H)\text{-}\rho_{xy}(-\mu_0 H)]/2$). To make sure the robustness of our measured results, different batches of samples were used to verify repeatedly.

III. RESULTS AND DISCUSSION

m-Cr_5Te_8 single crystals have monoclinic structures with the space-group $C_{2/m}$ (No. 12) as shown in Figs. 1(a) and 1(b). The crystal structure is related to the NiAs type with full and deficient metal layers stacking every second along the c axis. The Cr atoms are in an octahedral environment of Te anions occupying four unique crystallographic sites [14]. Cr_1 and Cr_4 atoms are located in the partially occupied metal atom layers with a site occupancy of 0.64 and 0.18, whereas Cr_2 and Cr_3 atoms are fully occupied [16]. Figure 1(c) shows the XRD pattern of a m-Cr_5Te_8 single crystal. Only (00l) Bragg peaks are detected, indicating that the exposed crystal surface is the ab plane. The full width at half-maximum (FWHM) of the (002) Bragg peak is 0.09° and a typical crystal size of flakelike shape m-Cr_5Te_8 single crystals is about $3 \times 2.5 \times 0.2$ mm^3 as presented in the inset of Fig. 1(c). The monoclinic crystal structure was confirmed by the Rietveld refinement of the powder XRD pattern of crushed single crystals [Fig. 1(d)] at room temperature with fitted lattice parameters $a = 13.644(2)$ Å, $b = 7.8377(1)$ Å, $c = 12.115(2)$ Å, and $\beta = 90.634(5)°$, in agreement with the reported literature [33].

In order to systematically investigate the magnetic properties of m-Cr_5Te_8 single crystals, we performed the measurements of magnetization as a function of temperature $M(T)$ and applied magnetic fields $M(\mu_0 H)$ along the c axis and the ab plane. Figures 2(a) and 2(b) show $M(T)$ under zero-field-cooled (ZFC) modes in the magnetic fields $\mu_0 H = 0.01$, 0.1, and 1 T for the $H \parallel c$ axis and the $H \parallel ab$ plane, respectively. The magnetization in two directions has almost an order of magnitude difference in the same magnetic field and the decrease of low-temperature magnetization below T_C can be suppressed in 1 T along the c axis whereas there still exists a decrease along the ab plane, indicating an obvious

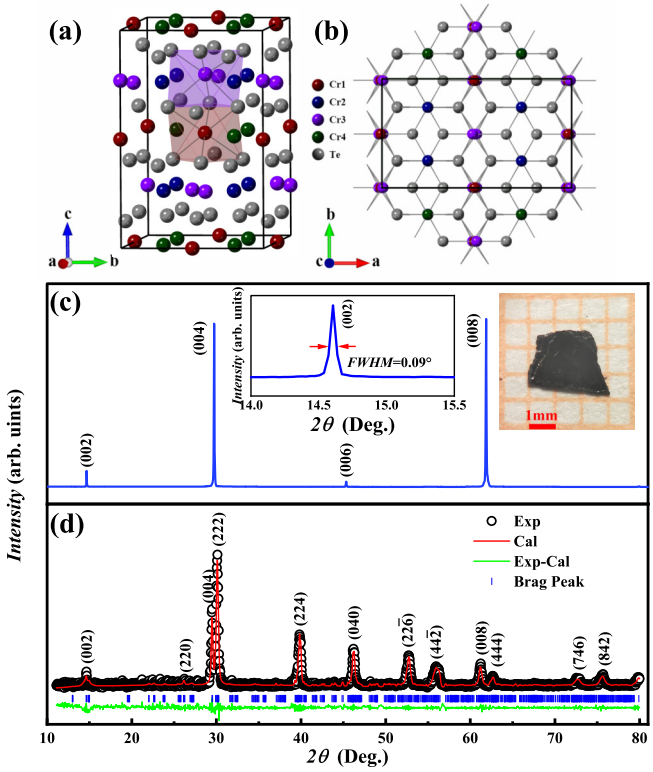

FIG. 1. (a) and (b) Crystal structures of m-Cr_5Te_8 observed from side view and top view. (c) XRD pattern of the single crystal measured on the (00l) surface. The insets present the typical x-ray curve of the (002) Bragg peak and the typical crystal size is about $3 \times 2.5 \times 0.2$ mm^3. (d) Rietveld refined powder XRD patterns at room temperature for crushed m-Cr_5Te_8 crystals. The vertical marks (blue bars) stand for the position of the Bragg peaks, and the solid line (green line) at the bottom corresponds to the difference between experimental and calculated intensities.

magnetic anisotropy. As shown in Fig. 2(c), there are sharp upturns for the $M(T)$ curves under different measuring modes. The T_Cs, defined as the temperatures where the minimum of dM/dT occurs, are 186 K for the $H \parallel ab$ plane and the $H \parallel c$ axis both. The resistivity ρ_{xx} on the ab plane shows a metallic behavior with a residual resistivity ratio of 3 and a kink was observed at T_C. As shown in the inset, $\rho_{xx}(T)$ at low temperatures can be well fitted by the Fermi liquid (F-L) formula $\rho_{xx}(T) = AT^2 + \rho_0$, which implies that the electron-electron scattering is dominant at low temperatures. Meanwhile, ZFC and field-cooled (FC) curves split significantly below T_C, which shows a spin-glass-like behavior [34]. It can be ascribed to the appearance of a canted antiferromagnetic (AFM) magnetic structure, with a large FM component along the c axis and a small AFM component along the ab plane according to the neutron-diffraction experiment [15,35]. Extraordinary, this process is accompanied by a sizable "thermohysteresis" between the field-cooled warming (FCW) and the field-cooled cooling (FCC) curves as shown in the green rectangle area, in a small temperature range below T_C, which is different from the previously reported results of m-Cr_5Te_8 since T_C varies greatly caused by the vacancy [15]. The thermohysteresis was observed obviously along the c axis. And the kinks show up in all three curves and can be suppressed in higher fields suggest the existence of contribution from both FM and AFM orders. The similar phenomenon has also been observed in Fe_3GeTe_2. Overall, it can be explained as the delaying response of the introducing of AFM interactions during cooling and warming processes [36].

To explore the possible reason for the anisotropy of the magnetization parallel and perpendicular to the c axis, we performed the measurement of angular-dependent magnetization. Figure 2(d) shows the out-of-plane magnetization $M(\varphi)$ at $T = 5$ K with the field rotated from the ab plane to the c axis, then back to the ab plane. It can be seen that the $M(\varphi)$ curves show simple twofold symmetries in the magnetic fields of 0.1, 0.3, 0.5, and 1 T, indicating that there exists an uniaxial anisotropy between the c axis and the ab plane. The magnetization exhibits the minimum when the $H \parallel ab$ plane and it reaches the maximum when the $H \parallel c$ axis, which confirms that the easy axis of magnetization is the c axis. It is deserved to note that in the magnetic field up to 1 T, $M(\varphi)$ curves do not present the obvious circular shape, which means the magnetic field is not sufficient to overcome the energy of magnetocrystalline anisotropy. In other words, the strong uniaxial anisotropy plays an important role in the magnetic anisotropy of m-Cr_5Te_8 [37].

Pressure, as a clean adjustment means, can accurately control the crystal lattice and the corresponding physical properties. To investigate the pressure effect, we applied hydrostatic pressure on m-Cr_5Te_8. Figure 2(e) presents a typical temperature dependence of ZFC magnetization $M(T)$ in the magnetic field 0.01 T under various hydrostatic pressures. With increasing pressure from 0 to 1 GPa, T_C decreases obviously from 186 to 137 K. The inset shows ZFC curves of releasing pressure to 0 GPa (gray line) and normal pressure (black line). Since there are no significant differences of the $M(T)$ curves between them, it can be deduced that no collapse of the crystal structure occurred and the structure can restore almost completely after the release of pressure. The detailed hydrostatic pressure dependence of T_C is as shown in Fig. 2(f). It can be found that T_C decreases linearly when the pressure increases. And the value of the pressure derivate dT_C/dP remains nearly constant ~ -50 K GPa^{-1}, dominating a remarkable change and tunability. The rate of variation of T_C is defined as $\Delta T/T = [T_C(P = 0\ \text{GPa})\text{-}T_C(P = n\ \text{GPa})]/T_C(P = 0\ \text{GPa})$, where n is the value of the pressure applied on the single crystal [38,39]. $\Delta T/T$ can reach up to 26% under the pressure of 1 GPa, which demonstrates that the strong spin-lattice coupling from the view of active lattice modulation in m-Cr_5Te_8 [39]. As the pressure increases, we assume that the c axis exhibits a remarkable contraction whereas the a and b axes show a small expansion with decreasing temperature. The contraction of the c axis leads to a reduction of the Cr-Cr distance between layers implying stronger AFM interactions [15,34]. The effective exchange interactions J_{eff} consists of the majority positive (J_+) and the minority negative (J_-) ones. Consequently, the contraction of the c axis due to pressure gives rise to a decrease in the ratio J_+/J_-, which may result in the decrease in T_C [19,40]. Moreover, an obvious hysteresis in $M(\mu_0 H)$ was observed when the pressure reaches to 1 GPa and the details were as shown in Supplemental Material Fig. S2 [32].

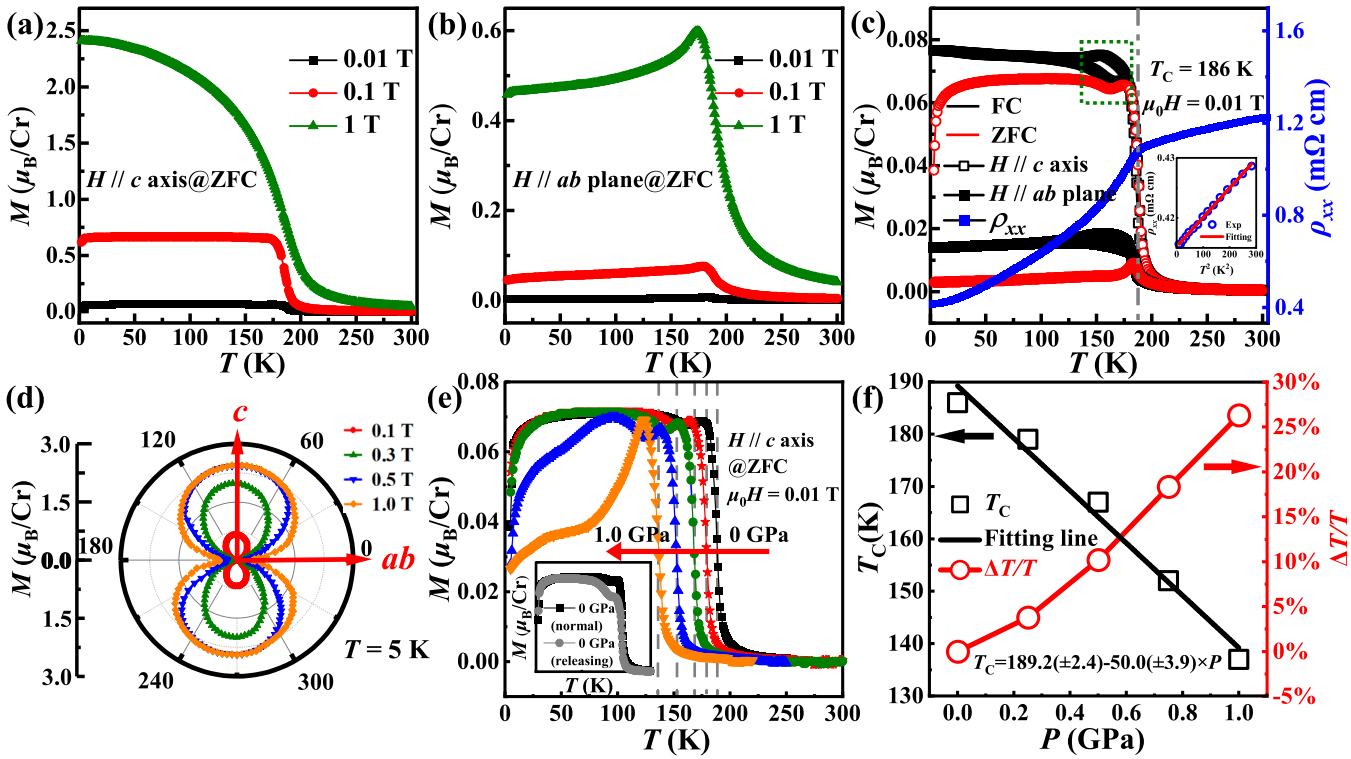

FIG. 2. (a) and (b) The temperature dependence of the magnetization of m-Cr_5Te_8 under ZFC modes in the applied field $\mu_0 H = 0.01$, 0.1, and 1 T. (c) The temperature dependence of the magnetization in $\mu_0 H = 0.01$ T under the ZFC (red line) and FC (black line) modes along the c axis and the ab plane separately and the bump area is highlighted using the green rectangle. The variation of the resistivity in $\mu_0 H = 0$ T with respect to temperature (blue line) was also plotted here, and the inset shows the F-L fitting of ρ_{xx}. (d) The angular-dependent magnetization at different angles for $T = 5$ K, and the applied fields are 0.1, 0.3, 0.5, and 1 T, respectively. (e) Typical temperature dependence of magnetization under ZFC modes in $\mu_0 H = 0.01$ T for various pressures from 0 to 1 GPa. The inset shows the $M(T)$ curves of releasing pressure to (gray line) and normal pressure (black line). (f) Evolution of T_C and $\Delta T/T$ under various pressures.

As follows from Figs. 3(a)–3(f), the magnetic anisotropy of m-Cr_5Te_8 also behaves as the anisotropy magnetocaloric effect (MCE). According to the classical thermodynamic theory and the Maxwell equations, the isothermal magnetic entropy change $\Delta S_M(T,H)$, induced by a variation of the external magnetic-field ΔH, can be expressed as below [41,42],

$$\Delta S_M(T,H) = S_M(T,H) - S_M(T,0) \tag{1}$$

$$= \int_0^H \left[\frac{\partial M(T,H)}{\partial T}\right]_H dH. \tag{2}$$

For magnetization measured in small discrete magnetic fields and temperature intervals, $\Delta S_M(T,H)$ could be practically approximated as below,

$$\Delta S_M(T,H) = \frac{\int_0^H M(T_{i+1},H)dH - \int_0^H M(T_i,H)dH}{T_{i+1} - T_i} \tag{3}$$

$$= \frac{\int_0^H M(T_{i+1},H)dH - \int_0^H M(T_i,H)dH}{\Delta T}, \tag{4}$$

where $M(T_i,H)$ and $M(T_{i+1},H)$ are the magnetization at T_i and T_{i+1} temperatures, respectively, in the same magnetic field H. $T = T_i + \Delta T/2$ or $T = T_{i+1} - \Delta T/2$. Based on the initial isothermal $M(\mu_0 H)$ curves near T_C [Figs. 3(a) and 3(b)], the calculated $-\Delta S_M(T,H)$ as a function of temperature in various fields up to 4.5 T along the c axis and the ab plane are depicted in Figs. 3(c) and 3(d). As expected, all curves exhibit broad peaks around T_C, whereas $-\Delta S_M$ reaches to the maximum $\sim$2.8 J kg^{-1} K^{-1} along the c axis and $\sim$1.8 J kg^{-1} K^{-1} along the ab plane. Furthermore, $-\Delta S_M$ increases with increasing the change in magnetic fields ΔH, which is comparable with the normal MCE material at a second-order FM phase transition. But for the $H \parallel ab$ plane, the temperature dependence of $-\Delta S_M$ exhibits anomalous behavior at fields below 2 T where positive values of ΔS_M are found. This anomalous behavior originates from the competition between the temperature dependence of magnetic anisotropy and the magnetization, similar to VI_3 [43]. The rotational magnetic entropy change $-\Delta S_M^R$ can be expressed as the difference of $-\Delta S_M$ between the c axis and the ab plane: $\Delta S_M(T,H_c)$-$\Delta S_M(T,H_{ab})$. As shown in Fig. 3(e), $-\Delta S_M^R$ also shows a peak at T_C, changing from 0.4 J kg^{-1} K^{-1} to 1.1 J kg^{-1} K^{-1}. With increasing fields, the maximum of $-\Delta S_M^R$ moves away from T_C to lower temperatures, which might stem from a strong temperature dependency of magnetic anisotropy [27]. Additionally, the field-dependent $-\Delta S_M$ with fields along the c axis and the ab plane are also as shown in Fig. 3(f) and both of them present upward trends. It is interesting to note that some values of $-\Delta S_M$ for the ab plane are negative in low fields. However, all the values are positive along the c axis, indicating that a MCE anisotropy exists in the m-Cr_5Te_8 system.

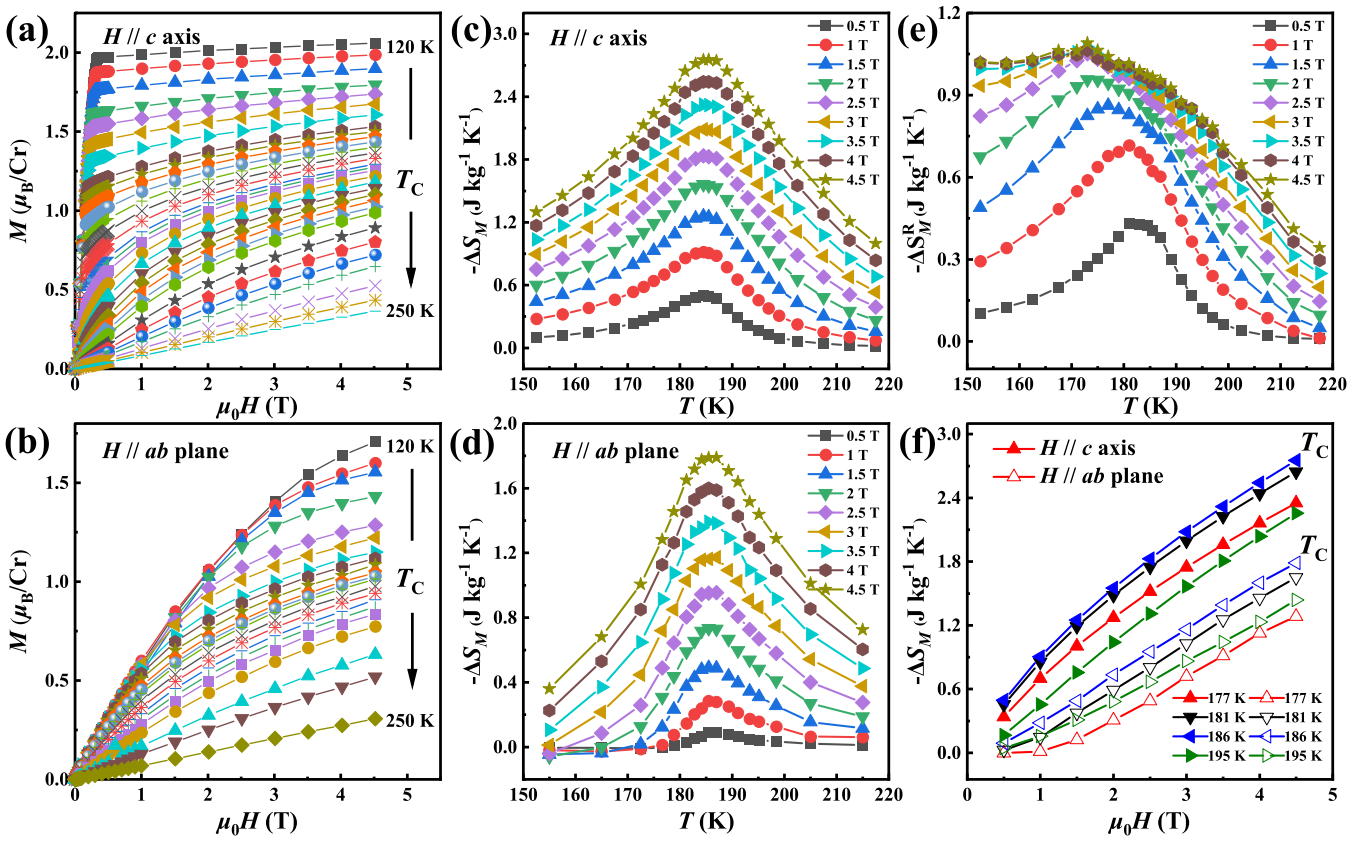

FIG. 3. The magnetic-field dependence of the magnetization $M(\mu_0 H)$ for (a) the $H \parallel c$ axis and (b) the $H \parallel ab$ plane. The temperature dependence of $-\Delta S_M(T, H)$ in different fields for (c) the $H \parallel c$ axis and (d) the $H \parallel ab$ plane. (e) The temperature dependence of $-\Delta S_M^{\mathrm{R}}(T, H)$ in different fields. (f) The magnetic-field dependence of $-\Delta S_M(T, H)$ at different temperatures for the $H \parallel c$ axis and the $H \parallel ab$ plane.

As to AHE, it is unlike the ordinary Hall effect (OHE) owing to the path bending of charge carriers caused by Lorentz force perpendicular to the magnetic field. The AHE, mostly appearing in FM materials, can be observed with no requirement of an applied magnetic field to cause deflection of charge carriers. The total Hall resistivity ρ_{xy} is the superposition of the ordinary Hall resistivity ρ_{xy}^{O} and the anomalous Hall resistivity ρ_{xy}^{A}, which can be expressed by the empirical formula as below [44],

$$\rho_{xy} = \rho_{xy}^{\mathrm{O}} + \rho_{xy}^{\mathrm{A}} = R_0 B + R_{\mathrm{S}} \mu_0 M, \tag{5}$$

where R_0 and R_{S} are the ordinary and anomalous Hall coefficients, respectively. B is related to the magnetic-field H by $B = \mu_0(H\text{-}N_{\mathrm{d}}M)$, where N_{d} is the demagnetization factor, μ_0 is the vacuum permeability, and M is the magnetization. A method devoted to calculating in a rectangular FM prism was used with detailed analysis given in Ref. [45]. And we calculated that N_{d} is 0.7 in our system.

Figure 4(a) presents the magnetic-field dependence of the Hall resistivity $\rho_{xy}(B)$ at 5 K with the $H \parallel c$ axis. With rising magnetic fields, ρ_{xy} decreases rapidly first and reaches a maximum in $\mu_0 H \sim 0.38$ T, corresponding well with saturated magnetic fields as shown in Fig. 5(a). And then it starts to increase as the magnetic fields increase. These results demonstrate that there exist AHE in m-Cr_5Te_8. In high fields, the magnetization is saturated. Thus, the spontaneous part of the Hall effect is a constant, and the observed variation of ρ_{xy} with fields is mainly due to OHE. Additionally, with falling magnetic fields, ρ_{xy} could overlap well with rising one in addition to $H \sim 0.26$ T as shown in the inset. The kink or inconsistency indicates there may exist a spin-flop process induced by magnetic fields, and the possible reasons will be discussed herein below. It should be stressed that we have investigated different single crystals taken from different batches, and this novel property can be well repeated in all measured single crystals. Figure 4(b) shows the magnetic-field dependence of the Hall resistivity $\rho_{xy}(B)$ at different temperatures with falling fields. We can obtain the value of the ordinary Hall coefficient R_0 and the anomalous Hall resistivity ρ_{xy}^{A} from the linear fit of ρ_{xy} curves at the saturation region. The slope and the intercept of the y axis is corresponding to R_0 and ρ_{xy}^{A}, respectively. Moreover, the anomalous Hall coefficient R_{S} can be obtained by using the formula $\rho_{xy}^{\mathrm{A}} = R_{\mathrm{S}}\mu_0 M_{\mathrm{S}}$ with M_{S} taken from different isothermal $M(\mu_0 H)$ curves in $\mu_0 H = 1$ T. As shown in Fig. 4(c), the values of R_0 are all positive, confirming that the hole-type carriers are dominant. The derived carrier concentration $n = -1/e/R_0$ in the inset of Fig. 4(c) increases abruptly around T_{C} with a maximum value of 9.75×10^{20} cm^{-3} due to the possible change in Fermi surface [26]. Meanwhile, as shown in Fig. 4(d), R_{S} is two orders of magnitude larger than R_0 as reported in other literature [26,46–49]. Another behavior to be noted is that R_{S} decreases monotonously with decreasing temperature and almost keeps zero at 105 K, then it goes to be negative. The temperature T_{M}

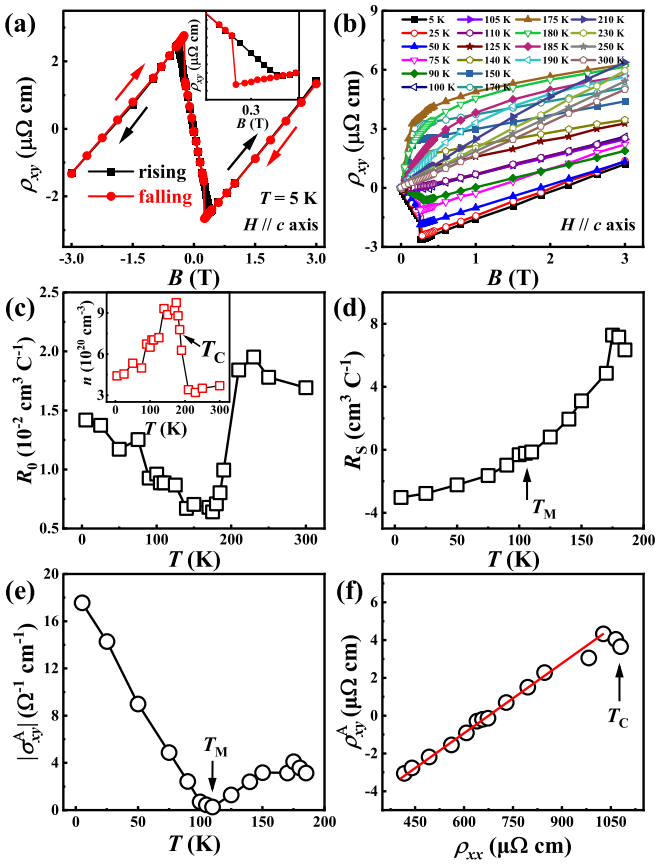

FIG. 4. The Hall measurement of the m-Cr_5Te_8 single crystal. The magnetic field dependence of the Hall resistivity ρ_{xy} at (a) $T = 5$ K (the red line represents the measurement process with a falling magnetic field whereas the black line means a rising one, and the inset shows an abnormity around 0.26 T) and (b) different temperatures along the c axis. (c) The ordinary Hall coefficient R_0, (d) anomalous Hall coefficient R_S, and (e) anomalous Hall conductivity ρ_{xy}^A as a function of temperature. The inset of (c) presents the derived carrier concentration $n(T)$. (f) The plot of ρ_{xy}^A versus ρ_{xx} with the linear fit (solid red line) below T_C.

is defined here where the sign of R_S changes. According to Fig. 2(c), the $M(T)$ curve under ZFC modes presents a broad maximum around T_M with the $H \parallel c$ axis. It means that the FM coupling is the dominant interaction in m-Cr_5Te_8; however, a certain number of AFM couplings create substantial frustration [50]. This peculiar spin configuration, resulting in a competitive relationship between FM and AFM, may play an important role in the transport properties of the Hall resistivity.

Figure 4(e) presents the temperature-dependent anomalous Hall conductivity $\sigma_{xy}^A (\approx \rho_{xy}^A/\rho_{xx}^2 = R_S\mu_0 M/\rho_{xx}^2)$. Theoretically, the intrinsic contribution of σ_{xy}^A is the order of $e^2/(ha)$, where e is the electronic charge, h is the Plank constant, and a is the lattice parameter [51]. Taking $a = V^{1/3} \sim 10.7$Å (V = 1275.6839Å^3), σ_{xy}^A is about 361 Ω^{-1}cm^{-1}, which is much bigger than the calculated σ_{xy}^A, precluding the possibility of an intrinsic mechanism. Figure 4(f) exhibits the scaling behavior of ρ_{xy}^A and ρ_{xx}. A clear linear relationship was observed, further precluding the side-jump mechanism. This observation leads us to determine that the skew-scattering mechanism is the most likely cause of AHE in m-Cr_5Te_8 with a scaling behavior of $\rho_{xy}^A = \beta\rho_{xx}$ usually used to describe a symmetric scattering induced by impurity or defect [52,53].

We have noted that, during the measurement of the Hall resistivity, an abnormal jump of ρ_{xy} occurred. It can also be observed in $M(\mu_0 H)$ and $M(T)$ curves [Figs. 5(a) and 5(b)] only with the $H \parallel c$ axis. Below T_C, as the magnetic field decreases to around 0.26 T, we can see a sharp decrease in the magnetization in $M(\mu_0 H)$ curves. Likewise, near 0.26 T, we can also note a sharp decrease in magnetization in $M(T)$ curves as the temperature decreases. Similar phenomena can be seen in the measurement of ac susceptibility as shown in Fig. S3 of the Supplemental Material [32] too. To further explore this phenomenon, we define several related parameters, M_S, H_S, H_C, and $M \times H$. As shown in Fig. 5(c), M_S represents saturation magnetization corresponding to the high field. H_S is defined as the saturated magnetic field where the saturation magnetization just reached or magnetization curves separate. With decreasing fields, the magnetization changes suddenly at a critical point, and the applied magnetic field at this time is defined as H_C. The value of the hysteresis loss $M \times H$ is depicted as the area of the red triangular region in this figure. Figure 5(d) shows the temperature dependence of these parameters. For H_C, it shows a relatively low value when the temperature is close to $T_C \sim 186$ K. As the temperature decreases further, H_C increases quickly and tends to be a constant 0.26 T. At the same time, H_S shows a monotonically increase as the temperature decreases. The similar trend occurs in the M_S curve. Due to stronger magnetic exchange interactions at low temperatures, usually accompanied by a higher saturation magnetization, it increases with decreasing temperature first and then stays unchanged when the temperature is low enough. $M \times H$ increases monotonically as well since it depends on the former three parameters' common changing circumstances. To evaluate the degree of changes, the mutation ratio $R = (M_B\text{-}M_A)/M_B$ is used. Here, M_B represents for the magnetization before the jump just the same as M_S, and M_A represents for the magnetization after the jump. As shown in Fig. 5(d), a maximum value of R about 0.3(30%) occurs around 5 K, and it is worth noting that the jump is steep occurring in a tiny field range about 0.0025 T during our measurements. In addition, at high temperatures close to T_C, the jump behavior disappears and R is close to zero. By the way, we also grew other Cr-based compounds with different T_Cs which show different results, indicating a T_C dependence of the mutation ratio R (Figs. S4 and S5 of the Supplemental Material [32] and Refs. [54,55]).

In order to further investigate the origin of the jump behavior in m-Cr_5Te_8, the possible magnetic structures without Te atoms have been drawn. Based on the measurement of the neutron scattering from the study of Huang *et al.* [35], Fig. 5(e) presents the magnetic excited-state (left figure) and the magnetic ground-state (right figure) structures. Concentrating on the crystal structure of m-Cr_5Te_8 as shown in Fig. 1(a), Cr_1 and Cr_3 atoms as well as Cr_2 and Cr_4 atoms centered octahedra share common faces. It means that there is a strong overlap of Cr $3d_{z^2}$-Cr $3d_{z^2}$ along the crystallographic c direction with a relatively smaller nearest-neighbor Cr-Cr distance leading to AFM exchange interactions [25,28]. Within the ab plane, the Cr-Cr distances are longer than 3.75 Å and thus there are

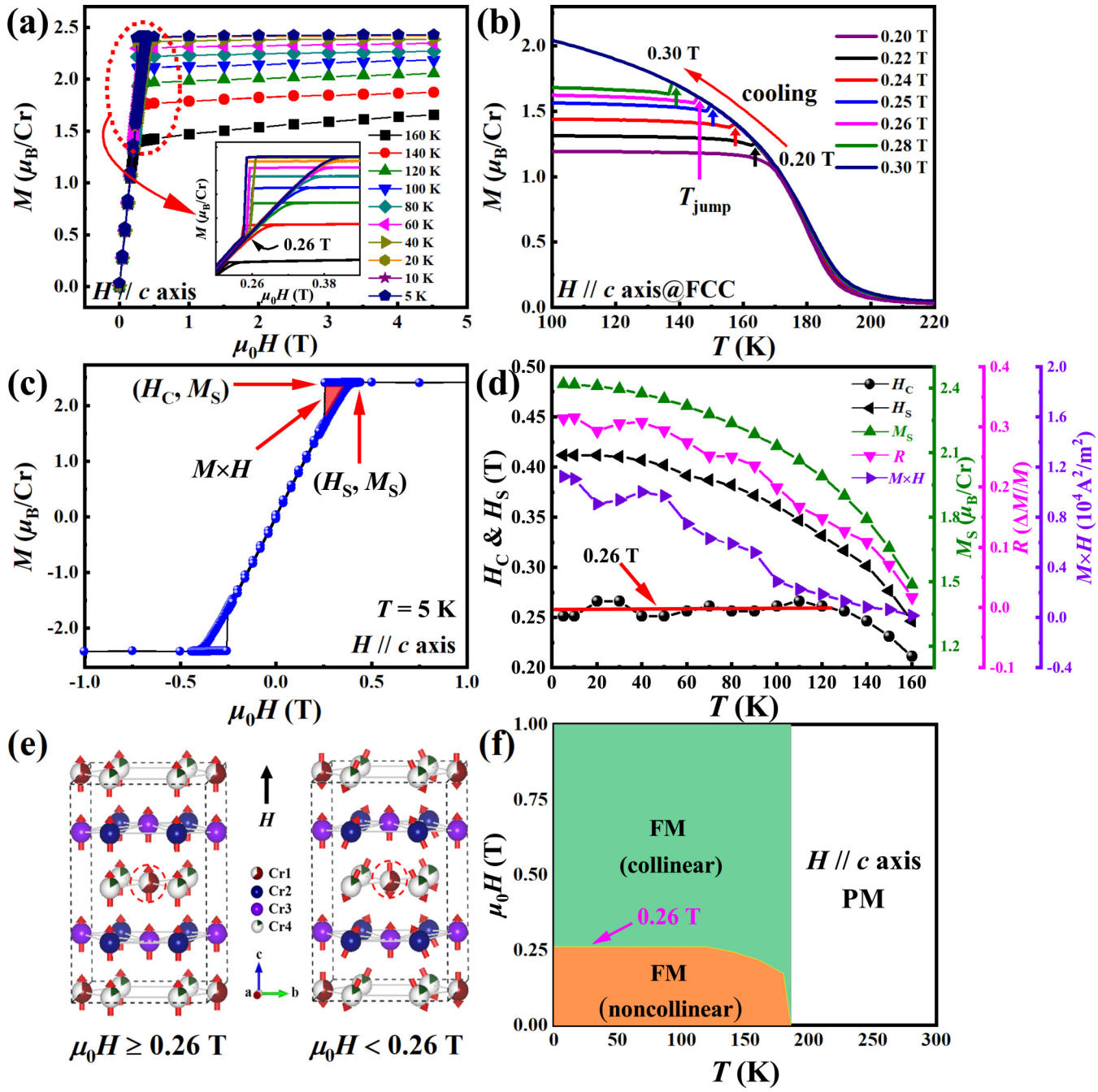

FIG. 5. (a) The magnetization curves in the first quadrant at different temperatures, showing jumps as illustrated in the inset. (b) FCC curves in different magnetic fields around 0.26 T. (c) Hysteresis loop at 5 K. M_S, H_S, H_C, and $M \times H$ are defined here in this figure. (d) Different parameters as a function of temperature. The (e) possible magnetic structures and (f) phase diagram of m-Cr_5Te_8. Cr_1 atoms are in red and white, Cr_4 atoms are in green and white (white represents the proportion of unoccupied parts), and Cr_2, Cr_3 atoms are separately in blue and purple.

no direct interactions. FM superexchange interactions occurs in the layer via near 90° Cr-Te-Cr bonding which links a half-filled t_{2g} on one Cr atom with an empty e_g level on the other Cr atom [25,50]. Therefore, when the magnetic field is larger than 0.26 T, the spins are all aligned in one direction well. As the magnetic field decreases until 0.26 T, the AFM coupling emerges, and the spin of the Cr_1 atom in the red circle starts to reverse. Simultaneously, with the generation of the metastable state and energy accumulation, it becomes unstable and then the spin arrangements of surrounding Cr_1 atoms tilt up. Finally, a sudden drop of the magnetic moment occurs. As shown in Fig. 5(b), it is reasonable that collinear Cr spins under FCC modes are metastable due to the competition between AFM and FM exchange interactions. Around 0.26 T, when the temperature decreases to the separation temperature T_{jump}, the accumulation of the potential energy of the metastable state is so large that Cr spins switch to flop. Thus, the magnetization in FCC curves drops back to FCW curves.

The metastable state is induced by the applied magnetic field, and if the field is too small to induce or too large to keep the stability, jumping behaviors will vanish [56]. This behavior is different from the previous reports on $NbFeO_3$ [57] and $SmFeO_3$ [58] single crystals where the changes in magnetization are caused by the spin reorientation and appear in ZFC curves. However, the metamagnetic transition in m-Cr_5Te_8 is irreversible and occurs in FCC curves (see for more details and analysis in Figs. S6 and S7 of the Supplemental Material [32]). Moreover, the magnetic phase diagram with the $H \parallel c$ axis was also obtained based on our observations. As shown in Fig. 5(f), for $T > T_C$, m-Cr_5Te_8 shows PM behavior, and when $T \leqslant T_C$, it presents FM behavior. Furthermore, for $T \leqslant T_C$, the collinear-FM state and the noncollinear-FM state are switched below and above the critical field ~0.26 T.

IV. CONCLUSION

To summarize, we experimentally grew the m-Cr_5Te_8 single crystals by the mixed-flux method. We have systematically investigated the magnetic properties of m-Cr_5Te_8 single crystals through the measurements of angular-dependent magnetization, hydrostatic pressures, magnetic entropy change, and AHE. A large anisotropy between the c axis and the ab plane was found, and the mechanism of AHE was revealed by a series of analyses including scaling relationships, which possibly originates from the skew-scattering mechanism rather than the intrinsic or side-jump mechanism. Meanwhile, the experimental results showed T_C is sensitive to the pressure, indicating remarkable adjustability. Moreover, the spin-flop behavior was observed around 0.26 T, and its possible origin was discussed. Correspondingly, the magnetic phase diagram was also obtained. However, it remains unclear what does the real magnetic structure look like and why do other chromium tellurides with similar structures not show a similar jump. As they have not yet been determined in our studies, further investigations of the magnetic properties in m-Cr_5Te_8 are of great interest and urgently needed. The suitable critical magnetic field and the significant rate of change make it a potential candidate for magnetic-switch devices. Due to recent progress on controllably synthesized ultrathin Cr_nX (X = S, Se, and Te; $0 < n < 1$), our results might also be helpful for exploring the future spintronics or other electronic device applications of this kind of material, considering that it can become a possible new platform for investigating 2D magnetism.

ACKNOWLEDGMENTS

This work was supported by the National Key Research and Development Program under Contract No. 2016YFA0300404 and the National Nature Science Foundation of China under Contracts No. 11674326, No. 11874357, and No. 11904003 and the Joint Funds of the National Natural Science Foundation of China and the Chinese Academy of Sciences' Large-Scale Scientific Facility under Contracts No. U1832141 and No. U1932217 and the Key Research Program of Frontier Sciences, CAS (Grant No. QYZDB-SSW-SLH015) and The uses with Excellence and Scientific Research Grant of Hefei Science Center of CAS (Grant No. 2018HSC-UE011).

[1] N. D. Mermin and H. Wagner, Phys. Rev. Lett. **17**, 1133 (1966).
[2] X. X. Li and J. L. Yang, J. Mater. Chem. C **2**, 7071 (2014).
[3] W. B. Zhang, Q. Qu, P. Zhu, and C. H. Lam, J. Mater. Chem. C **3**, 12457 (2015).
[4] M. A. McGuire, H. Dixit, V. R. Cooper, and B. C. Sales, Chem. Mater. **27**, 612 (2015).
[5] M. Yi and Z. G. Shen, J. Mater. Chem. A **3**, 11700 (2015).
[6] C. X. Huo, Z. Yan, X. F. Song, and H. B. Zeng, Sci. Bull. **60**, 1994 (2015).
[7] V. Carteaux, D. Brunet, G. Ouvrard, and G. Andre, J. Phys.: Condens. Matter **7**, 69 (1995).
[8] C. Gong, L. Li, Z. L. Li, H. W. Ji, A. Stern, Y. Xia, T. Cao, W. Bao, C. Z. Wang, Y. Wang, Z. Q. Qiu, R. J. Cava, S. G. Louie, J. Xia, and X. Zhang, Nature (London) **546**, 265 (2017).
[9] B. Huang, G. Clark, E. Navarro-Moratalla, D. R. Klein, R. Cheng, K. L. Seyler, D. Zhong, E. Schmidgall, M. A. McGuire, D. H. Cobden, W. Yao, D. Xiao, P. Jarillo-Herrero, and X. D. Xu, Nature (London) **546**, 270 (2017).
[10] Y. J. Deng, Y. J. Yu, Y. C. Song, J. Z. Zhang, N. Z. Wang, Z. Y. Sun, Y. F. Yi, Y. Z. Wu, S. W. Wu, J. Y. Zhu, J. Wang, X. H. Chen, and Y. B. Zhang, Nature (London) **563**, 94 (2018).
[11] M. Bonilla, S. Kolekar, Y. J. Ma, H. C. Diaz, V. Kalappattil, R. Das, T. Eggers, H. R. Gutierrez, M. H. Phan, and M. Batzill, Nat. Nanotechnol. **13**, 289 (2018).
[12] Y. Zhang, J. W. Chu, L. Yin, T. A. Shifa, Z. Cheng, R. Q. Cheng, F. Wang, Y. Wen, X. Y. Zhan, Z. X. Wang, and J. He, Adv. Mater. **31**, 1900056 (2019).
[13] J. Dijkatra, H. H. Weitering, C. F. van Bruggen, C. Haas, and R. A. de Groot, J. Phys.: Condens. Matter **1**, 9141 (1989).
[14] Y. Liu and C. Petrovic, Phys. Rev. B **96**, 134410 (2017).
[15] X. Zhang, T. L. Yu, Q. Y. Xue, M. Lei, and R. Z. Jiao, J. Alloys Compd. **750**, 798 (2018).
[16] W. Ben and C. Niither, Mater. Res. Bull. **32**, 305 (1997).
[17] H. Ipser, K. Komarek, and K. Klepp, J. Common Met. **92**, 265 (1983).
[18] A. Berg, Ph.D. thesis, University of Oslo, 1950; cited in F. Grønvold and E. F. Westrum, Zeitschrift für anorganische und allgemeine Chemie **328**, 272 (1964).
[19] K. Hatakeyama, T. Kaneko, H. Yoshida, S. Ohta, and S. Anzai, J. Magn. Magn. Mater. **90**, 175 (1990).
[20] K. Oda, S. Yoshii, Y. Yasui, M. Ito, T. Ido, Y. Ohno, Y. Kobayashi, and M. Sato, J. Phys. Soc. Jpn. **70**, 2999 (2001).
[21] T. Hamasaki and T. Hashimoto, Solid Sate Commun. **16**, 895 (1975).
[22] K. O. Klepp and H. Ipser, Angew. Chem. Int. Ed. Engl. **21**, 911 (1982).
[23] M. A. McGuire, V. O. Garlea, S. Kc, V. R. Cooper, J. Yan, H. Cao, and B. C. Sales, Phys. Rev. B **95**, 144421 (2017).
[24] H. Ipser, Monatsh. Chem. **111**, 761 (1980).

[25] K. Lukoschus, S. Kraschinski, C. Näther, W. Bensch, and R. K. Kremer, J. Solid State Chem. **177**, 951 (2004).
[26] Y. Liu and C. Petrovic, Phys. Rev. B **98**, 195122 (2018).
[27] X. H. Luo, W. J. Ren, and Z. D. Zhang, J. Magn. Magn. Mater. **445**, 37 (2018).
[28] R. Mondal, R. Kulkarni, and A. Thamizhavel, J. Magn. Magn. Mater. **483**, 27 (2019).
[29] Y. H. Wang, J. Yan, J. B. Li, S. S. Wang, M. Song, J. P. Song, Z. H. Li, K. Chen, Y. L. Qin, L. S. Ling, H. F. Du, L. Cao, X. Luo, Y. M. Xiong, and Y. P. Sun, Phys. Rev. B **100**, 024434 (2019).
[30] C. A. Juillerat, V. V. Klepov, G. Morrison, K. A. Pace, and H. C. zur Loye, Dalton Trans. **48**, 3162 (2019).
[31] M. Morishita, F. Kawamura, T. Iwahashi, M. Yoshimura, Y. Mori, and T. Sasaki, Jpn. J. Appl. Phys. **42**, L565 (2003).
[32] See Supplemental Material at http://link.aps.org/supplemental/10.1103/PhysRevB.102.144433 for sample characterization, field dependence of the magnetization under pressure, ac susceptibility measurement, and metastable state analysis.
[33] T. Tsuji and K. Ishida, Thermochim acta **253**, 11 (1995).
[34] J. Wontcheu, W. Bensch, S. Mankovsky, S. Polesya, and H. Ebert, Prog. Solid State Chem. **37**, 226 (2009).
[35] Z. L. Huang, W. Kockelmann, M. Telling, and W. Bensch, Solid State Sci. **10**, 1099 (2008).
[36] J. Y. Yi, H. L. Zhuang, Q. Zou, Z. M. Wu, G. X. Cao, S. W. Tang, S. A. Calder, P. R. C. Kent, D. Mandrus, and Z. Gai, 2D Mater. **4**, 011005 (2016).
[37] M. Akram and F. M. Nazar, J. Mater. Sci. Lett. **2**, 441 (1983).
[38] J. Cheng and J. Luo, J. Phys.: Condens. Matter **29**, 383003 (2017).
[39] Y. Sun, R. C. Xiao, G. T. Lin, R. R. Zhang, L. S. Ling, Z. W. Ma, X. Luo, W. J. Lu, Y. P. Sun, and Z. G. Sheng, Appl. Phys. Lett. **112**, 072409 (2018).
[40] S. Ohta, J. Phys. Soc. Jpn. **54**, 1076 (1985).
[41] K. A. Gschneidner Jr, V. K. Pecharsky, and A. O. Tsokol, Rep. Prog. Phys. **68**, 1479 (2005).
[42] X. Yu, X. Zhang, Q. Shi, S. Tian, H. Lei, K. Xu, and H. Hosono, Front. Phys. **14**, 43501 (2019).
[43] J. Yan, X. Luo, F. C. Chen, J. J. Gao, Z. Z. Jiang, G. C. Zhao, Y. Sun, H. Y. Lv, S. J. Tian, Q. W. Yin, H. C. Lei, W. J. Lu, P. Tong, W. H. Song, X. B. Zhu, and Y. P. Sun, Phys. Rev. B **100**, 094402 (2019).
[44] C. M. Hurd, *The Hall Effect in Metals and Alloys* (Plenum, New York, 1972).
[45] A. Aharoni, J. Appl. Phys. **83**, 3432 (1998).
[46] Q. Wang, S. S. Sun, X. Zhang, F. Pang, and H. C. Lei, Phys. Rev. B **94**, 075135 (2016).
[47] Y. H. Wang, C. Xian, J. Wang, B. J. Liu, L. S. Ling, L. Zhang, L. Cao, Z. Qu, and Y. M. Xiong, Phys. Rev. B **96**, 134428 (2017).
[48] J. Yan, X. Luo, F. C. Chen, Q. L. Pei, G. T. Lin, Y. Y. Han, L. Hu, P. Tong, W. H. Song, X. B. Zhu, and Y. P. Sun, Appl. Phys. Lett. **111**, 022401 (2017).
[49] J. Yan, X. Luo, G. T. Lin, F. C. Chen, J. J. Gao, Y. Sun, L. Hu, P. Tong, W. H. Song, Z. G. Sheng, W. J. Lu, X. B. Zhu, and Y. P. Sun, Europhys. Lett. **124**, 67005 (2018).
[50] Z. L. Huang, W. Bensch, D. Benea, and H. Ebert, J. Solid State Chem. **178**, 2778 (2005).
[51] S. Onoda, N. Sugimoto, and N. Nagaosa, Phys. Rev. Lett. **97**, 126602 (2006).
[52] J. Smit, Physica **24**, 39 (1958).
[53] D. Yue and X. F. Jin, J. Phys. Soc. Jpn. **86**, 011006 (2017).
[54] Y. Liu and C. Petrovic, Phys. Rev. B **97**, 014420 (2018).
[55] G. T. Lin, X. Luo, F. C. Chen, J. Yan, J. J. Gao, Y. Sun, W. Tong, P. Tong, W. J. Lu, Z. G. Sheng, W. H. Song, X. B. Zhu, and Y. P. Sun, Appl. Phys. Lett. **112**, 072405 (2018).
[56] W. Y. Zhao, S. X. Cao, R. X. Huang, Y. M. Cao, K. Xu, B. J. Kang, J. C. Zhang, and W. Ren, Phys. Rev. B **91**, 104425 (2015).
[57] S. J. Yuan, W. Ren, F. Hong, Y. B. Wang, J. C. Zhang, L. Bellaiche, S. X. Cao, and G. Cao, Phys. Rev. B **87**, 184405 (2013).
[58] S. X. Cao, H. Z. Zhao, B. J. Kang, J. C. Zhang, and W. Ren, Sci. Rep. **4**, 5960 (2015).